Universal Output Characteristics of Single-Mode Operation in Low-Loss Large-V-Number Multimode Waveguide Lasers with Transverse Spatial Hole Burning

Chaofan Wang, Fatemeh HadavandMirzaee, and Tsing-Hua Her*

Department of Physics and Optical Science, The University of North Caroline at Charlotte, Charlotte, North Carolina 28223, USA

(Received 14 October 2019; revised manuscript received 27 December 2019; accepted 15 January 2020; published 18 February 2020)

We study the performance limit of single-mode operation in low-loss large-V-number planar waveguide lasers, with transverse spatial hole burning as the dominating mechanism for transverse-mode competition. By introducing normalized variables, we develop a simple semianalytical model to describe the universal output characteristics of single-mode emission before the onset of high-order modes, which can be easily scaled to a wide range of laser configuration parameters. Our model is validated using exact numerical solutions, which show applicability beyond that of the low-loss approximation. Our analysis establishes a minimum criterion of the loss ratio between the fundamental and first higher-order mode for a robust single-mode operation. This criterion is much weaker than that of conventional wisdom based on the pure wave-propagation argument, which we attribute to a resonator enhancement effect. Our universal outcome can be denormalized to establish the relationship between single-mode extraction efficiency and optimum output coupling in a multimode laser with arbitrary modal loss ratios over a wide range of single-pass unsaturated gain and loss.

DOI: 10.1103/PhysRevApplied.13.024042

I. INTRODUCTION

One of the fundamental questions in laser resonator physics is how to optimize the laser output power by balancing gain and loss in the resonators [1–4]. For a given set of gain and internal loss (such as scattering and absorption due to the gain medium and optical components at the laser frequency), optimal laser efficiency can be obtained by selecting the appropriate external coupling loss provided by the output coupler. A prototypical example is a homogeneously saturated laser resonator with a uniform transverse spatial intensity profile (i.e., a truncated plane wave). In the absence of longitudinal spatial hole burning and with the assumption of low internal loss, simple dependences of optimum extraction efficiency and output coupling on the unsaturated gain and internal loss can be analytically derived [see, for example, Eq. (9)] [5]. For arbitrary levels of gain and loss, Rigrod pointed out in 1978 that this question was analytically intractable [1]. This was later solved numerically by Schindler [2], who displayed the optimum efficiency and corresponding output coupling conveniently at the intersection of contour lines of the single-pass unsaturated gain and single-pass distributive loss of interest (hereafter, we refer to this as Schindler's plot). Although the plane-wave laser model is rudimentary, Schindler's plot elucidates general trends of laser resonator behavior to provide a simple first-order guidance on laser-performance optimization. For example, very high efficiency can only be obtained with very low distributive loss and small output coupling; modest efficiency with high loss would require a very large single-pass gain and large output coupling. In the high-gain and high-loss regime, the laser becomes insensitive to output coupling.

Modern lasers, on the other hand, are mostly waveguide-based for high efficiency, compactness, stability, and superior beam quality. In particular, large-mode-area leaky waveguides, in the form of slabs [6], channels [7], or fibers [8], attract significant attention for high-power scaling. For such lasers, higher-order modes (HOMs) can oscillate due to transverse spatial hole burning (TSHB), leading to undesirable mode competition that deteriorates the output quality. Considerable efforts are devoted to waveguide design to suppress HOM propagation by increasing the modal loss contrast between competing modes to make the waveguide effectively single mode [7,9–12]. Specifically, Li *et al.* proposed a loss discrimination criterion of less than 0.1 dB/m for the fundamental mode (FM) and 100 × higher for the first HOM in coiled step-index fibers [13], while experimentally a modal loss ratio of a few hundred [14] or even thousands [15] has been demonstrated. This criterion, however, is reasoned based on a pure propagation effect

*ther@uncc.edu

in fiber amplifiers and does not consider the optical feedback inherent in lasers. Concurrently, steady-state mixed-state operation in fiber lasers and amplifiers, involving transverse-mode competition, is reported [16–19]. These studies, however, are mostly numerical and only investigate a very limited configuration space of gain, loss, cavity length, and mirror reflectivity. An analytical model that considers all four variables in the widest possible parameter space does not yet exist. We note that, even though transverse-mode competition due to TSHB is no longer the roadblock in contemporary high-power lasers [20–22], it remains a major challenge for single-mode (SM) operation in multimode waveguide lasers (MMWLs).

The purpose of this paper is to study the performance limit of steady-state single-mode operation in low-loss large-V-number planar waveguide lasers, with transverse spatial hole burning as the dominating mechanism for transverse-mode competition. We are not concerned with instability in mixed-state dynamics in MMWLs, where strong mode competition among multiple transverse modes is present [23,24]. For our study, at least four parameters must be considered: single-pass loss of the FM and the first HOM, single-pass unsaturated gain, and output coupling. The interplay among these parameters is far from trivial. By introducing normalized variables to reduce the number of unknowns, we develop a simple semianalytical model to describe universal output characteristics of single-mode emission before the onset of high-order modes in MMWLs. Upon denormalization, our results can be easily scaled to a wide range of laser configuration parameters. We validate our model using exact numerical solutions, which show applicability beyond that of the low-loss approximation. Our analysis establishes a minimum criterion of the modal loss ratio between the fundamental and first higher-order modes for a robust single-mode operation. This criterion is much weaker than that of conventional wisdom based on a pure wave-propagation argument, which we attribute to a resonator enhancement effect. Our universal outcome can be denormalized to produce Schindler's plots with arbitrary modal loss ratios over a wide range of single-pass unsaturated gain and loss, which will be very useful for the design and operation of SM large-mode-area waveguide lasers.

II. BASIC FORMALISM

We consider a generic planar step-index large-V-number waveguide with a core width d and a length L that is sandwiched between two flat reflectors, R_l and R_r, at the left-hand ($z=0$) and right-hand ($z=\mathrm{L}$) ends of the resonator, respectively. A large V number implies large modal confinement [25], which allows us to consider only the field in the core. We consider only the FM ($n=1$) and first HOM ($n=2$), each of which has a modal loss coefficient of α_n, modal power of $P_n(z)$, and normalized intensity profiles $f_n(x)$ where $f_1(x)=2\cos^2(\pi x/d)/d$ and $f_2(x)=2\sin^2(2\pi x/d)/\mathrm{d}$ [26]. The pump excitation is assumed to generate a uniform electronic population inversion in the core that interacts with signal photons in both modes via stimulated emission, leading to gain saturation by the sum of the modal intensities. For simplicity, we assume that both modes oscillate at the line center. This assumption does not actually reduce the generality of the analysis, since off-center frequencies can be represented by including a Lorentzian frequency factor in the gain coefficients, g_0, and saturation parameters, s, which equal the inverse of the saturation intensity [27]. The forward- (I_n^+) and backward- (I_n^-) propagating average intensities, defined by $I_n^{\pm}(z)=P_n^{\pm}(z)/d$, are governed by the following set of four coupled first-order nonlinear integrodifferential equations [26,28]:

$$\frac{dI_n^{\pm}}{dz}=\pm g_0 I_n^{\pm}\int_{-d/2}^{d/2}\frac{f_n(x)}{\left[1+sd\sum_{i=1}^{2}f_i(x)(I_i^{+}+I_i^{-})\right]}dx\mp\alpha_n I_n^{\pm}. \tag{1}$$

It can be straightforward to show that the threshold gain of oscillation is $g_1^{\mathrm{th}}L=\alpha_1 L-1/2\ln R_l R_r$ for the FM and

$$g_2^{\mathrm{th}}\int_0^L\left\{\int_{-d/2}^{d/2}\frac{f_2(x)}{[1+sdf_1(x)(I_1^{+}+I_1^{-})]}dx\right\}dz=\alpha_2 L-\frac{1}{2}\ln R_l R_r, \tag{2}$$

for the 1st HOM [28]. The ratio of the modal loss of these two modes is denoted as $k=\alpha_2/\alpha_1$.

A. Intrinsic single-mode operation

An intrinsically SM waveguide is characterized by an infinite k. Equation (1) can be simplified to become a set of two coupled first-order nonlinear ordinary differential equations [29]:

$$\frac{dI_1^{\pm}}{dz}=\pm g_0 I_1^{\pm}\left[\frac{1}{s(I_1^{+}+I_1^{-})}\times\left\{1-\frac{1}{[1+2s(I_1^{+}+I_1^{-})]^{1/2}}\right\}\right]\mp\alpha I_1^{\pm}. \tag{3}$$

In a low-loss and low-gain laser oscillator, the sum of the forward- and backward-propagating wave intensities are approximately equal, and one can replace the term $I_1^{+}(z)+I_1^{-}(z)$ by a constant, $2I$. For steady-state oscillation, where the round-trip gain must equal the round-trip

loss, we have

$$2g_0L\left[\frac{1}{2sI}\left(1-\frac{1}{\sqrt{1+4sI}}\right)\right]=2\alpha_1L-\ln R_lR_r, \quad (4)$$

from which the steady-state internal intensity, I, can be obtained

$$sI=\frac{1}{2}\left(r-\frac{1+\sqrt{1+8r}}{4}\right), \quad (5)$$

where $r=g_0L\big/(\alpha_1L-1/2\ \ln R_lR_r)$ is commonly known as the threshold parameter. In an optimized system, one of the mirrors would be close to unity and, without loss of generality, we assume $R_l=1$. To reduce the number of unknowns, we introduce a normalized gain parameter, $\gamma=g_0L\big/\alpha_1L$, and a normalized external loss (or external output coupling) parameter, $\tau=-1/2\ \ln R_r\big/\alpha_1L$, with which the FM threshold gain reduces simply to $\gamma_1^{\rm th}=1+\tau$ and the threshold parameter becomes $r=\gamma\big/\gamma_1^{\rm th}$ [27]. The normalized output intensity can be calculated according to $sI_{\rm out}=sI^+(L)(1-R_r)$, and the extraction efficiency at the low-loss limit then becomes

$$\eta_1\equiv\frac{sI^+(L)(1-R_r)}{g_0L}\approx\frac{-\ln R_r}{g_0L}sI=\frac{\tau}{\gamma}\left(r-\frac{1+\sqrt{1+8r}}{4}\right). \quad (6)$$

In Eq. (6), we employ the approximation $1-R\approx-\ln R$, which is valid for $R\geq 0.7$ and is consistent with the low-loss limit. According to Eq. (6), the output intensity can then be rewritten as $sI_{\rm out}=\eta_1g_0L$.

Equation (6) is plotted in Fig. 1(a) for a large set of normalized gains. An upper limit of $\tau=100$ is used on the x axis, corresponding to 4% reflectivity (i.e., a cleaved glass fiber end) with $\alpha_1L=0.02$. We note that $\gamma=1000$ is likely to be the practical upper limit, which corresponds to a very large single-pass gain of $gL=10$, with a relatively small single-pass loss, $\alpha_1L=0.01$. For the hypothetical case of an infinite gain (the top curve), it is straightforward to show from Eq. (6) that $\lim_{\gamma\to\infty}\eta_1=\tau\big/(1+\tau)$. All η_1 curves rise sharply at small τ, reach a maximum at an optimum value of $\tau_{\rm opt}$, and return to zero when the laser is overloaded at the lasing threshold, $\tau_{\rm th}=\gamma-1$. We note that $\tau_{\rm opt}$ is very well defined for $\gamma<1000$, which can be found by setting the derivative of Eq. (6) to zero, yielding

$$\gamma=\frac{(1+\tau_{\rm opt})}{16}\left[(\tau_{\rm opt}+3)\left(\tau_{\rm opt}+5+\sqrt{\tau_{\rm opt}^2+10\tau_{\rm opt}+9}\right)-8\right]. \quad (7)$$

Equation (7) can be alternatively interpreted as an optimum gain, $\gamma_{\rm opt}$, as a function of τ, which is plotted in Fig. 1(b), indicating that the required normailzed gain for optimum operation rises very quickly with τ. The corresponding optimum extraction efficiency is [from Eq. (6)]

$$\eta_1^{\rm opt}=(z-1)(z-4)^2\big/(z-2)^3, \quad (8)$$

where $z=1+\sqrt{1+8r_{\rm opt}}$ is defined to simplify the notation. Equation (8) is added to Fig. 1(a) as a solid red line. Equations (5)–(8) represent the generic laser equations for low-loss intrinsically SM large-V-number waveguide lasers, and Fig. 1 displays their universal behavior, regardless of the internal loss. The validity of Eqs. (5)–(8) is verified against the exact solution by solving Eq. (3) numerically with the proper boundary conditions [29]. As an example, Appendix A shows that Eq. (8) is fairly accurate for α_1L up to 0.5 over the output coupling range of $0.01<R<0.998$, even though the approximation $1-R\approx-\ln R$ is valid only for $R\geq 0.7$.

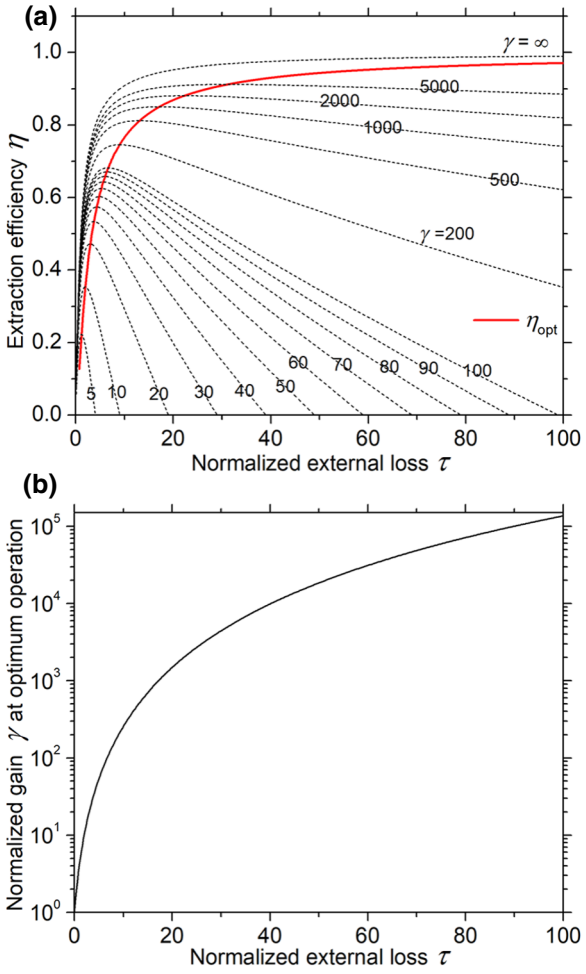

FIG. 1. (a) Extraction efficiency of intrinsic SM waveguide lasers as a function of the normalized external coupling loss for various normalized gains. The red solid line represents the optimum operation. (b) Optimum normalized gain as a function of the external coupling loss [from Eq. (7)].

Equations (5)–(8) are qualitatively similar to those for a low-loss plane-wave oscillator, which have the following simpler forms [5]:

$$\begin{aligned} sI &= \tfrac{1}{2}(r-1), \\ \ln R_{\text{opt}} &= -2\alpha L\left(\sqrt{\tfrac{g_0}{\alpha}}-1\right), \text{ or} \\ \tau_{\text{opt}} &= \sqrt{\gamma}-1, \text{ or } \gamma=(\tau+1)^2, \\ \eta_{\text{opt}} &= \left(1-\sqrt{\tfrac{\alpha}{g_0}}\right)^2 = \left(1-\tfrac{1}{\sqrt{\gamma}}\right)^2. \end{aligned} \tag{9}$$

Both platforms indicate that higher efficiencies require a larger normalized gain and normalized coupling loss, which is consistent with the practice of using a low-reflectivity output coupler (~4%–10%) in high-power lasers [7,8]. On the other hand, it is well known that, for a plane-wave oscillator, η_{opt} approaches unity at the limit of zero loss (in which case $\tau \to \infty$). It can be shown that, for this to happen, we have $\lim_{\tau\to\infty} \gamma/\tau \approx \tau$ [from Eq. (9)] and the internal loss scales with the external loss, according to

$$\alpha L \approx \frac{(\ln R)^2}{4gL} \propto (1-R)^2. \tag{10}$$

For large-V-number waveguide lasers, η_{opt} also approaches unity at the limit of zero loss [Eq. (8)], but the scaling is characteristically different. For this case, we have $\lim_{\tau\to\infty} \gamma/\tau \approx \tau^2$ [from Eq. (7)] and the internal loss scales with the external loss, according to

$$\alpha L \approx -\frac{(\ln R)^{3/2}}{(8gL)^{1/2}} \propto (1-R)^{3/2}. \tag{11}$$

This difference lies in the different degrees of saturation in the transverse direction of the gain media between these two types of lasers.

B. Single fundamental mode operation in multimode waveguide lasers

A MMWL is characterized by a finite loss ratio k. In this case, g_2^{th} is finite and represents the maximum unsaturated gain to sustain SM operation. For a low-loss resonator, $I_1^+(z)+I_1^-(z) \approx 2I$ and Eq. (2) is reduced to

$$\frac{2g_2^{\text{th}}L}{1+2sI+\sqrt{1+4sI}} = \alpha_2 L - \frac{1}{2}\ln R_l R_r, \tag{12}$$

while, at the same time, the FM satisfies Eq. (4) with a gain coefficient of g_2^{th}. Putting these together, one obtains an analytical expression of g_2^{th} in a normalized form,

$$\gamma_2^{\text{th}} = \frac{(\tau+k)(\tau+1)^2}{(\tau-k+2)^2} \quad \text{for } \tau \geq \tau_c = k-2, \tag{13}$$

where $\tau_c = k-2$ is defined as a critical point at which $\gamma_2^{\text{th}}(\tau_c)$ reaches infinity. Equation (13) is plotted in Fig. 2(a)

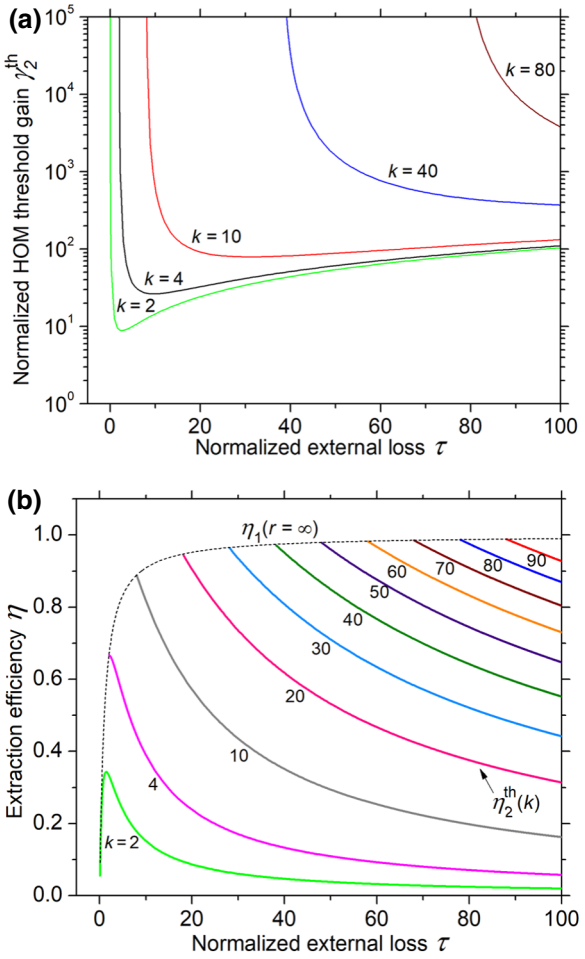

FIG. 2. (a) Normalized HOM threshold gain as a function of normalized external coupling loss for different modal loss ratios [Eq. (13)]. (b) Extraction efficiency η_2^{th} at HOM threshold for different modal loss ratios [Eq. (15)]. Each curve starts at the critical point, the loci of which corresponds to $\eta_1(\gamma=\infty)$.

for selected modal loss ratios. For $\tau \leq \tau_c$, the MMWL remains single mode, regardless of the gain, since the coupling loss is small enough for the FM to saturate the gain completely to prevent the HOM from oscillating. For $\tau > \tau_c$, the MMWL is single mode below the curve and multimode otherwise. Along this HOM threshold curve, the internal intensity, sI_2^{th}, can be found from Eq. (5) to be

$$sI_2^{\text{th}} = \frac{(k-1)(\tau+1)}{(\tau+2-k)^2} \quad \text{for } \tau \geq \tau_c, \tag{14}$$

and the corresponding extraction efficiency at the HOM threshold becomes [from Eq. (6)]

$$\eta_2^{\text{th}} \approx \frac{2\tau}{\gamma_2^{\text{th}}} sI_2^{\text{th}} = \frac{2(k-1)}{\tau+(k/\tau)+(k+1)} \quad \text{for } \tau \geq \tau_c. \tag{15}$$

Equation (15) is plotted in Fig. 2(b) for selected loss ratios. All η_2^{th} curves start at the critical points, the loci

of which, therefore, match nicely with the $\lim_{\gamma\to\infty}\eta_1$ curve [Eq. (6)]. Each curve has a well-defined maximum value near or at the critical point and decays with increasing τ. It can be shown from Eq. (15) that $\eta^{\rm th}_{2,\rm max}$ occurs at

$$\tau_{\rm max} = \begin{array}{ll} \sqrt{k}, & \text{for } \sqrt{k} \geq k-2 \text{ or } k \leq 4 \\ k-2=\tau_c, & \text{for } \sqrt{k} \leq k-2 \text{ or } k \geq 4 \end{array} \quad (16)$$

Substituting Eq. (16) into Eq. (15) yields

$$\eta^{\rm th}_{2,\rm max} = \begin{array}{ll} \dfrac{2(\sqrt{k}-1)}{\sqrt{k}+1}, & \text{for } k \leq 4 \\ \dfrac{k-2}{k-1}=\eta_c, & \text{for } k \geq 4 \end{array} . \quad (17)$$

For $k \geq 4$, the result is consistent with our previous report [28] and represents an asymptotic limit of the extraction efficiency. The validity of Eqs. (12)–(17) is verified against the exact solution by solving Eqs. (1) and (2) numerically with the proper boundary conditions [29]. As an example, Appendix A shows that Eq. (15) is fairly accurate for $\alpha_1 L$ up to 0.5 and over the output coupling range of $0.01 < R < 0.998$, even though the approximation $1-R \approx -\ln R$ is valid only for $R \geq 0.7$.

III. DISCUSSION

A. Basic strategy for higher SM efficiency in MMWLs

It is well known that, for an intrinsically SM waveguide laser (i.e., $k=\infty$), the smaller the loss, the larger the efficiency [see the $\eta_1^{\rm opt}$ curve in Fig. 1(a)]. For a multimode waveguide laser with a finite k, a very small α_1 is not necessarily advantageous, since α_2 is also small, such that the HOM can oscillate easily at high gains. The ideal strategy is to increase α_2 (and therefore, k) by waveguide design, while maintaining a small α_1. Unfortunately, in many cases, increasing α_2 unavoidably increases α_1 and reduces k. For example, increasing resonant tunneling of the HOM in a slab waveguide increases α_1 by 30 dB and reduces k by 20 times [9], while bending an optical fiber increases α_1 (linearly polarized $\rm LP_{01}$) by 50 dB and reduces k by 30 dB [13,17]. Why is a larger α_1 with a smaller k better than a smaller α_1 with a large k for SM operation in a MMWL? Our analytical theory can offer a simple insight.

Figure 3 summarizes the trends of η_1, $\eta_1^{\rm opt}$, and $\eta_2^{\rm th}$ curves. We assume the laser initially operates at a very large $\tau = 100$ due to a very low single-pass loss $\alpha_1 L$. If the laser is intrinsically single mode, then the extraction efficiency is $\eta_1(\gamma, \tau = 100)$, which can be fairly large, depending on the available gain. If the laser becomes multimode with a hypothetical loss ratio $k=20$ (a relatively small number is chosen here for the purpose of illustration, which is limited by the scope of Fig. 3), the gain can only go up to $\gamma_2^{\rm th} \sim 180$, with a relatively low efficiency of $\eta_2^{\rm th} \sim 0.3$ for SM emission. We assume enlarging the HOM loss increases $\alpha_1 L$ by 10 and reduces k by two. The SM operation then moves to $\tau = 10$ along the $\eta_2^{\rm th}(k=10)$ curve, which supports $\gamma_2^{\rm th} \geq 500$ with $\eta_2^{\rm th} \geq 0.8$ and increases the output intensity ($sI_{\rm out} = \eta_1 g_0 L$) by nearly sevenfold.

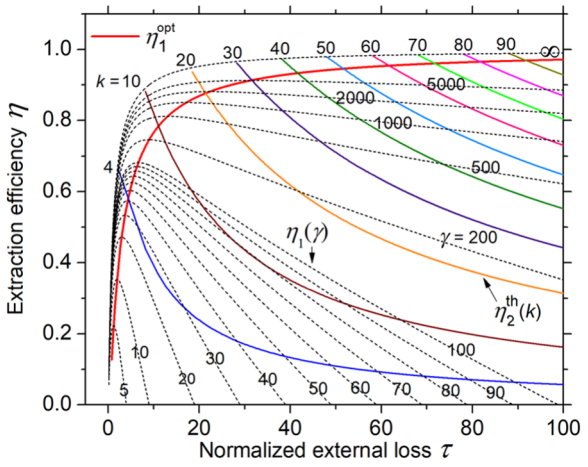

FIG. 3. Overlay of Figs. 1(a) and 2(b), displaying trends of η_1 (black dots), $\eta_1^{\rm opt}$ (red solid line), and $\eta_2^{\rm th}$ (colored solid lines, for $k \geq 4$) curves in normalized space.

B. Robust single-mode operation in multimode waveguide lasers

Figure 4 shows a simplified version of Fig. 3 for a generic modal loss ratio k. Below the long dash curve ($\lim_{\gamma\to\infty}\eta_1$) is the allowed operation zone, within which the

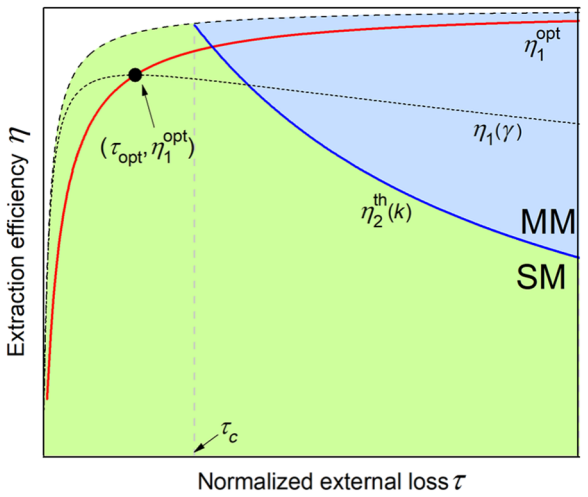

FIG. 4. Illustration of a robust SM operation, regardless of gain. Regions of operation are color-coded: white, forbidden; lime, SM; and blue, MM. $\eta_2^{\rm th}(k)$, $\eta_1^{\rm opt}$, and $\eta_1(\gamma)$ curves are represented by solid blue, solid red, and black dotted lines, respectively.

$\eta_2^{\text{th}}(k)$ curve separates the SM (below) and MM (above) zone. For a robust SM operation that is free of the HOMs, regardless of gain, the laser should have a normalized coupling parameter less than τ_c, which signals the starting point of the HOM threshold curve η_2^{th}. For a given normalized gain γ, the optimum normalized output coupling τ_{opt} [Eq. (7)] yields the highest efficiency η_1^{opt}[Eq. (8)], from which we propose the following criterion of minimum k for robust SM operation in planar MMWLs:

$$k \geq k_{\text{min}} = \tau_{\text{opt}}(\gamma) + 2. \tag{18}$$

In practice, a k value slightly larger than that of k_{min} may be beneficial to provide a safe margin during laser operation. This is consistent with the criterion set by Li *et al.* [13]: based on this number of $\alpha_1 < 0.1$ dB/m (or 0.023 1/m) for LP_{01} mode and $\alpha_2 \geq 10$ dB/m in a 5-m long fiber with a typical 4% output coupler of a cleaved fiber, τ is estimated to be about 15. If we allow for a fudge factor of two to account for the difference between two-dimensional (2D) fibers and one-dimensional (1D) slabs, we have $\tau \sim 30$. This suggests $k_{\text{min}} = \tau_{\text{opt}} + 2 = 32$, which is three times smaller than that of $k = 100$ reported by Li *et al*. This indicates a sizable difference in the required modal loss ratio between an amplifier and a laser. We interpret this reduction of k for lasers in terms of a resonator effect, where the optical feedback makes the effective cavity length longer to reduce the required k for the suppression of the HOMs.

C. Universal path for optimum SM operation in MMWLs and Schindler's plots

The above robust SM operation requires $\tau_{\text{opt}}(\gamma) \leq \tau_c$, which limits the extraction efficiency to $\eta_1^{\text{opt}}(\tau_c)$. As illustrated in Fig. 5, higher extraction effciency can be obtained by moving along the η_1^{opt} curve beyond τ_c until reaching the η_2^{th} curve, and then taking a left turn further along the η_2^{th} curve until the critical point. We denote this sickle-shaped trajectory as the universal path for the optimum SM operation, where the highest SM efficiency is sought for the given normalized gain. The intersection of the η_1^{opt} and η_2^{th} curves is denoted as the kink point, which is defined by Eqs. (7) and (13) to satisfy (for $\tau \geq \tau_c = k - 2$)

$$\begin{aligned}\gamma_{\text{kink}} &= \frac{(1+\tau_{\text{kink}})}{16}\left[(\tau_{\text{kink}}+3)\left(\tau_{\text{kink}}+5\right.\right.\\ &\left.\left.+\sqrt{\tau_{\text{kink}}^2+10\tau_{\text{kink}}+9}\right)-8\right]\\ &= \frac{(\tau_{\text{kink}}+k)(\tau_{\text{kink}}+1)^2}{(\tau_{\text{kink}}-k+2)^2}.\end{aligned} \tag{19}$$

For a modal loss ratio of $k = 4$, which is characteristic of an index-antiguided planar waveguide laser [28], our low-loss approximation yields $\tau_{\text{kink}} \approx 4.4$ and $\gamma_{\text{kink}} \approx 42.3$ [Eq. (19)], internal intensity $sI_{\text{kink}} \approx 2.79$ (Eq. (14)), threshold parameter $r_{\text{kink}} \approx 7.83$, and $\eta_{\text{kink}} \approx 0.58$ [Eqs. (8) or (15)]. The validity of these numbers is verified against the exact solution by solving Eqs. (1) and (2) numerically for different values of $\alpha_1 L$. Table I in Appendix A shows that η_{kink} is fairly accurate for $\alpha_1 L$ up to 0.5 and $0.01 < R < 0.998$, even though the approximation $1 - R \approx -\ln R$ is valid only for $R \geq 0.7$. Other laser parameters are reasonably accurate up to $\alpha_1 L = 0.3$ (within 10%).

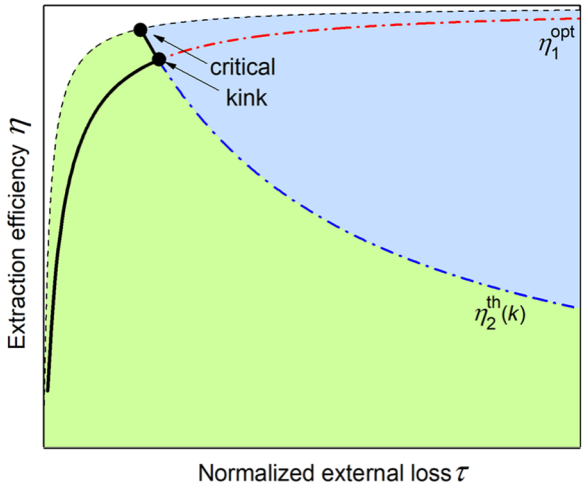

FIG. 5. Illustration of a universal path for the optimum SM operation (solid black curve), where the highest SM efficiency is sought for the given normalized gain. Regions of operation are color-coded: white, forbidden; lime, SM; and blue, MM.

Given a universal optimum path for a specific modal loss ratio k, denormalizing it for different values of $\alpha_1 L$ yields the Schindler's plot for that k-specific MMWL. Figures 6(a)–6(c) show the denormalized Schindler's plots for $k = 4$, 10, and 50, respectively. These are compared to those generated numerically [Fig. 10(a–b) in Appendix B], showing good quantitative agreement except in the regions of high loss and high gain ($\alpha_1 L > 0.3$ and $g_0 L > 5$), where the low-loss approximation no longer holds. For each plot, the red dashed lines represent the loci of kink points from different gain and loss contours, which have identical extraction efficiencies, as a consequence of this denormalization from the same universal path. Our theory explains why these kink points have the same extraction efficiency, which was first reported in Ref. [28] without clarification. Below the kink points, these contour lines in Fig. 10 are identical, indicating the lasers are intrinsically single mode, as the gain is small and the loss is too high for the HOM to oscillate. Above the kink points, these contour lines bend towards the critical point to avoid regions of high gain and small loss where the HOMs oscillate. Bending of the contour lines is most obvious for low k [Fig. 6(a)], but also exists at high k [the inset in Fig. 6(c)]. Figure 6 shows that η_{kink} and η_c increase with larger k,

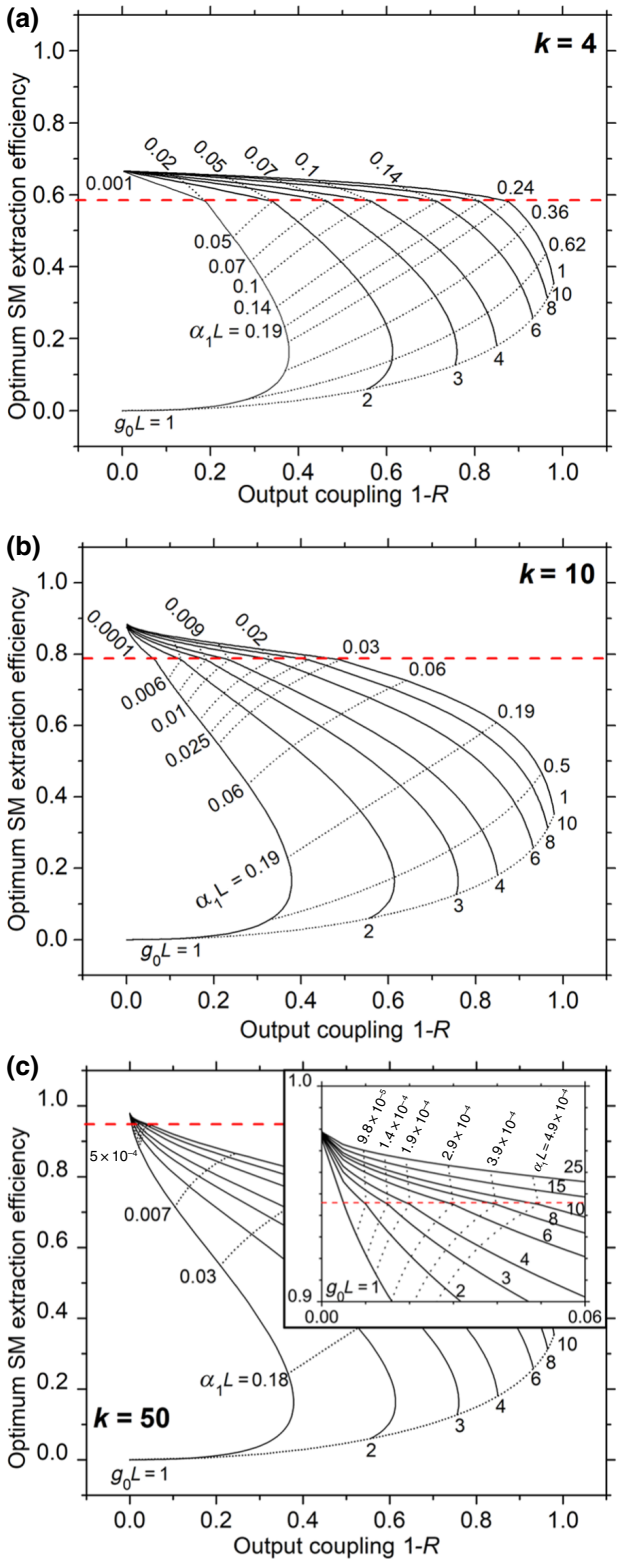

FIG. 6. Schindler's plots for (a) $k=4$, (b) $k=10$, and (c) $k=50$, obtained from denormalizing the universal optimum paths in Fig. 4(b). Solid and dotted black lines are contours of constant single-pass unsaturated gain and loss, respectively. The red dashed lines indicate the loci of the kink points. Inset in (c) is an expanded view near the apex, indicating bending of the contour lines is evident in this case.

indicating a larger operation space for SM operation. This is best understood from Fig. 3, where all universal optimum paths (i.e., sickle-shaped trajectories for different k) are displayed and compared. Figure 10(b) in Appendix B shows strong resemblance in Schindler's plots between $k=\infty$ and $k=50$, suggesting that $k=50$ is already more than enough for high-efficiency SM operation.

D. Scaling of laser performance with the modal loss ratio in MMWLs

It is useful to examine how various laser parameters scale with the modal loss ratio k in MMWLs where mode competition is dominated by TSHB. Since efficient lasers require low loss, this validates the low-loss assumption that underpins Eqs. (4)–(17). Figure 7(a) displays the k dependence of $\eta^{\text{th}}_{2,\text{max}}$ (solid red lines) and η_{kink} (dashed blue lines) on the left axis. Both quantities start equally at $k=2$, rise sharply, and saturate towards unity beyond $k=20$. They have maximum contrast near $k=10$, where $\eta^{\text{th}}_{2,\text{max}}$ and η_{kink} reach about 80% and 90% of their saturating values, respectively. Figure 7(a) also displays the k dependence of the corresponding τ_{max} [solid red

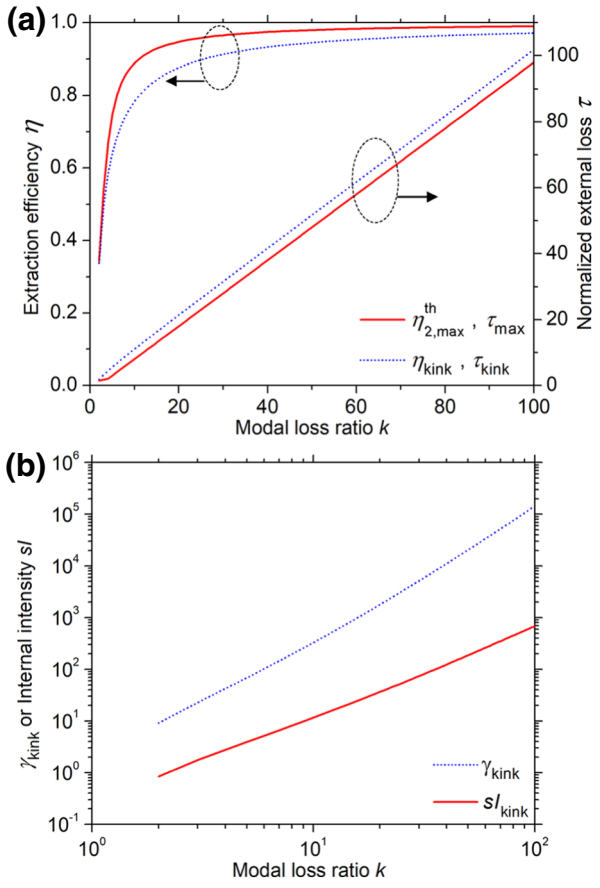

FIG. 7. (a) Extraction efficiency of $\eta^{\text{th}}_{2,\text{max}}$ and η_{kink} (left axis) and their corresponding τ_{max} and τ_{kink} (right axis), as a function of the modal loss ratio k. (b) k dependence of normalized gain γ_{kink} and normalized internal intensity sI_{kink} at kink points.

lines, Eq. (16)] and τ_{kink}[dashed blue lines, Eq. (19)] on the right axis. In the region of practical interest ($k \geq 4$), $\tau_{\text{max}} = \tau_c = k - 2$, while τ_{kink} can be fit reaonably well by $\tau_{\text{kink}} \approx k + 1$. Figure 7(b) shows a log-log plot of the k dependence of the normalized gain γ_{kink} [Eq. (19)] and normalized internal intensity sI_{kink} [Eq. (14)], indicating that both quantities rise sharply with k. For $k \geq 10$, our formulas [Eqs. (8), (14), (15), and (19)] yield the following scaling laws:

$$\begin{aligned} &\eta_{\text{kink}},\ \eta_c \propto k^0 \\ &\tau_{\text{kink}},\ \tau_c \propto k \\ &sI_{\text{kink}} \propto k^2 \\ &\gamma_{\text{kink}} \propto k^3 \\ &sI_{\text{out}} \propto k^3 \alpha_1 L. \end{aligned} \tag{20}$$

The last expression in Eq. (20) is obtained from $sI_{\text{out}} = sI_2^{\text{th}}(1 - R) \approx sI_2^{\text{th}} 2\tau\alpha_1 L$ with $\tau_{\text{kink}} \sim k$. Taken together, Fig. 7 and Eq. (20) indicate that large-k lasers require escalating higher gain ($\propto k^3$) and larger output coupling ($\propto k$) for optimum SM operation. The former may be practically limited by the availability of pump power or the onset of impairments, such as optical nonlinearities and/or thermal Rayleigh scattering (also known as modal instability) in the waveguides [20], while the latter is consistent with the use of low-reflectivity mirrors (4% for air-fiber or 30% for air-GaAs interfaces) in high-power lasers. Although increasing k does not improve extraction efficiency ($\propto k^0$), as it already approaches unity, it can substantially increase the output power ($\propto k^3$). From this persepctive, it is beneficial to have a larger k value for high-power SM operation.

IV. CONCLUSION

We present a semianalytical model to describe universal output characteristics of SM emission in one-dimensional low-loss large-V-number multimode waveguide lasers. This model uses normalized variables for a comprehensive analysis of SM operation, which can be easily scaled to the full parameter space. We validate our model with exact numerical solutions and demonstrate its wide applicability beyond the low-loss limit. Our analysis establishes a minimum criterion of modal loss contrast between competing modes for a robust SM operation. Our prediction is much weaker than that of conventional wisdom based on a pure propagation effect, which is a clear signature of optical feedback inherent in the laser resonators. Our universal outcome can be denormalized to generate Schindler's plots with arbitrary modal loss ratios over a wide range of single-pass unsaturated gain and loss with very good accuracy. Our current model can be, in principle, extended to large-mode-area waveguides with an arbitrary loss, smaller V number, or higher dimensionality (2D channels or fibers) by solving numerically a modified set of Eqs. (1) and (2) with proper boundary conditions. We expect that general observations and conclusions drawn from our current study will remain valid, which will be very useful for the design and operation of SM large-mode-area waveguide lasers.

ACKNOWLEDGMENTS

T.H. acknowledges Dr. Lee W. Casperson for many years of fruitful discussion, stimulating interaction, and sustained support. We thank the reviewers for suggesting a simplified form of Eq. (12). We also thank Mr. Joel Solomon and Mr. Joseph Obeid for proofreading the manuscript.

APPENDIX A: VALIDATION OF THE LOW-LOSS APPROXIMATION

Figure 8 displays the optimum extraction efficiency, η_1^{opt}, determined analytically from Eq. (8) (red circles) and numerically from Eq. (3) for different values of $\alpha_1 L$ (colored solid lines), as a function of normalized coupling loss parameter τ. Each numerical curve of a specific $\alpha_1 L$ is displayed with an output coupler reflectivity, R, between 0.998 (lower bound in τ) and 0.01 (higher bound in τ). The discrepancy near $R = 0.01$ increases with $\alpha_1 L$. For $\alpha_1 L$ up to 0.5, the overall discrepancy is not significant, even though the approximation $1 - R \approx -\ln R$ is technically accurate only for $R \geq 0.7$. Figure 8 demonstrates that Eq. (8) is fairly accurate for an internal loss of $\alpha_1 L$ up to 0.5. A low internal loss of $\alpha_1 L = 0.01$ shows excellent agreement with our analytical prediction.

Figure 9 shows the τ dependence of SM extraction efficiency at the HOM onset, η_2^{th}, for selected values of modal loss ratios, k, determined analytically from Eq. (15) (red circles) and numerically from Eqs. (1) and (2) for different values of $\alpha_1 L$ (color solid lines). Each numerical curve of a specific $\alpha_1 L$ is displayed with an output coupler reflectivity, R, between 0.998 (lower bound in τ) and 0.01 (higher bound in τ). The discrepancy near $R = 0.01$ in each

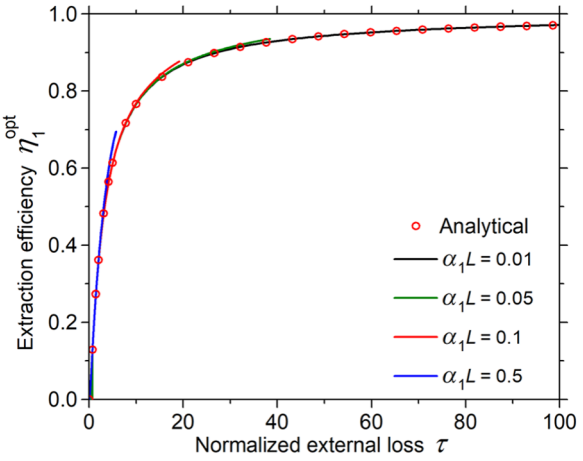

FIG. 8. Validation of Eq. (8) with exact numerical solutions for various single-pass losses.

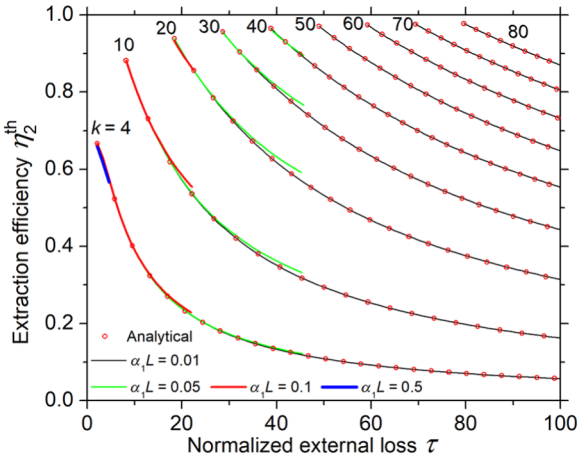

FIG. 9. Validation of Eq. (15) with exact solutions for various single-pass losses.

curve is small, even though the approximation $1-R \approx -\ln R$ is technically accurate only for $R \geq 0.7$. Figure 9 demonstrates that Eq. (15) is fairly accurate for an internal loss of $\alpha_1 L$ at least up to 0.5. A low internal loss of $\alpha_1 L = 0.01$ shows excellent agreement with our analytical prediction.

Table I displays the exact numerical solution [Eqs. (1) and (2)] of various laser parameters at the kink point for different values of internal losses $\alpha_1 L$ for a MMWL with $k = 4$. As a comparison, our low-loss approximation yields $\tau_{\text{kink}} \approx 4.4$ and $\gamma_{\text{kink}} \approx 42.3$ [Eq. (19)], internal intensity $sI_{\text{kink}} \approx 2.79$ [Eq. (14)], threshold parameter $r_{\text{kink}} \approx 7.83$, and $\eta_{\text{kink}} \approx 0.58$ [Eqs. (8) or (15)]. This shows that η_{kink} is fairly accurate for $\alpha_1 L$ up to 0.5 and $0.01 < R < 0.998$, even though the approximation $1-R \approx -\ln R$ is valid only for $R \geq 0.7$. Other laser parameters are reasonably accurate up to $\alpha_1 L = 0.3$ (within 10%).

APPENDIX B: VALIDATION OF THE SCHINDLER'S PLOTS AT LOW-LOSS APPROXIMATION

Here, we compare our denormalized Schindler's plots based on our semianalytical theory with those obtained numerically from Eqs. (1) and (2) with proper boundary conditions [28,29]. Figure 10(a) overlays a numerical Schindler's plot for $k = 4$ (red lines) and a denormalized Schindler's plot [black lines, from Fig. 6(a)]. Similarly,

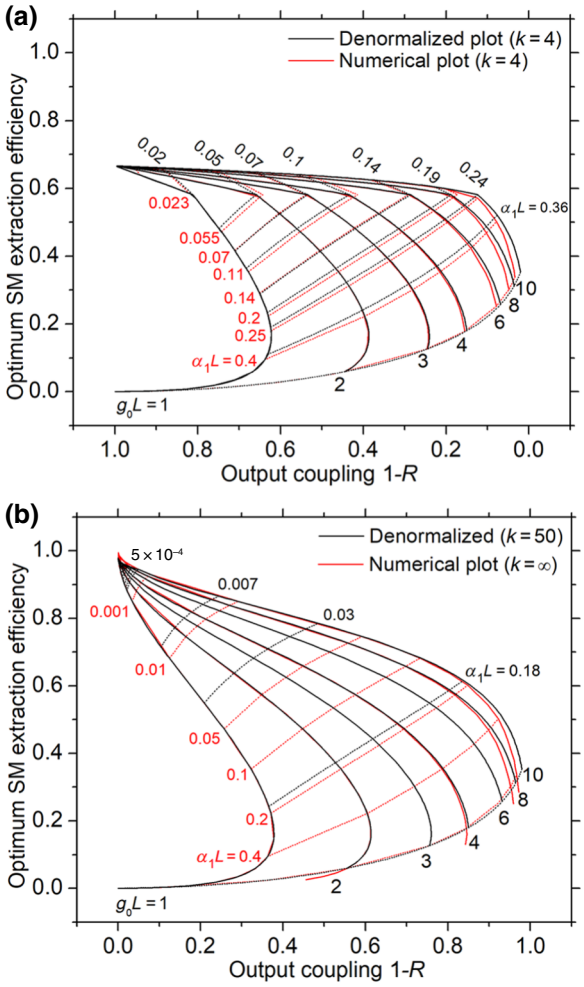

FIG. 10. (a) Overlay of Schindler's plot for $k = 4$ obtained numerically (red) and by denormalization (black). (b) Overlay of Schindler's plots for $k = \infty$ obtained numerically (red) and for $k = 50$ obtained by denormalization (black). The two plots have the same $g_0 L$, but different $\alpha_1 L$ values, so attention should be paid to constant-gain (i.e., vertical solid) contour lines.

TABLE I. Exact numerical solution of laser parameters at the kink point (for $k = 4$).

$\alpha_1 L$	$g_0 L$	R_{kink}	$\gamma_{\text{kink}} = g_0 L/\alpha_1 L$	$\tau_{\text{kink}} = -\ln(R_{\text{kink}})/2\alpha_1 L$	η_{kink}	r_{kink}	sI_{kink}
0.01	0.42	0.92	42.36	4.41	0.582	7.83	2.79
0.05	2.12	0.64	42.31	4.42	0.581	7.81	2.79
0.10	4.24	0.41	42.35	4.41	0.581	7.83	2.79
0.14	5.95	0.29	42.48	4.41	0.582	7.86	2.80
0.20	8.59	0.17	42.94	4.39	0.582	7.97	2.86
0.30	13.46	0.08	44.88	4.31	0.584	8.46	3.07
0.40	19.44	0.04	48.61	4.18	0.586	9.39	3.48
0.50	27.15	0.02	54.31	4.02	0.587	10.83	4.12

Fig. 10(b) overlays a numerical Schindler's plot for $k = \infty$ (red lines) and a denormalized Schindler's plot of $k = 50$ [black lines, from Fig. 6(c)]. The two plots in each figure have the same $g_0 L$ (solid lines), but different $\alpha_1 L$ (dotted line), so attention should be paid to constant-gain (i.e., solid vertical) contour lines. Figure 10 clearly shows that these two Schindler's plots have very good overall agreement, except at the lower-right corner (i.e., the high-loss and high-gain region), where the low-loss approximation no longer holds. Figure 10(b) displays an additional minor discrepancy near the apex, which is inherent between $k = \infty$ and $k = 50$. Overall, $k = 50$ very closely resembles $k = \infty$.

[1] W. Rigrod, Homogeneously broadened CW lasers with uniform distributed loss, Quantum Electronics, IEEE J. **14**, 377 (1978).

[2] G. Schindler, Optimum output efficiency of homogeneously broadened lasers with constant loss, Quantum Electronics, IEEE J. **16**, 546 (1980).

[3] F. Sanchez, B. Meziane, T. Chartier, G. Stephan, and P. L. François, Output-coupling optimization of Nd-doped fiber lasers, Appl. Opt. **34**, 7674 (1995).

[4] T. S. Mansuripur, G.-M. de Naurois, A. Belyanin, and F. Capasso, Lasers with distributed loss have a sublinear output power characteristic, Optica **2**, 48 (2015).

[5] A. E. Siegman, *Lasers* (University Science Books, Mill Valley, CA, 1986), Vol. 13.

[6] D. P. Shepherd, S. J. Hettrick, C. Li, J. I. Mackenzie, R. J. Beach, S. C. Mitchell, and H. E. Meissner, High-power planar dielectric waveguide lasers, J. Phys. D-Appl. Phys. **34**, 2420 (2001).

[7] J. N. Walpole, J. P. Donnelly, P. J. Taylor, L. J. Missaggia, C. T. Harris, R. J. Bailey, A. Napoleone, S. H. Groves, S. R. Chinn, R. Huang, and J. Plant, Slab-coupled 1.3-μm semiconductor laser with single-spatial large-diameter mode, IEEE Photonics Technol. Lett. **14**, 756 (2002).

[8] C. Jauregui, J. Limpert, and A. Tünnermann, High-power fibre lasers, Nat. Photonics **7**, 861 (2013).

[9] A. Kumar, V. Rastogi, and K. S. Chiang, Leaky optical waveguide for high power applications, Appl. Phys. B-Lasers Opt. **85**, 11 (2006).

[10] J. M. Fini, Design of solid and microstructure fibers for suppression of higher-order modes, Opt. Expr. **13**, 3477 (2005).

[11] K. Saitoh, N. J. Florous, T. Murao, and M. Koshiba, Realistic design of large-hollow-core photonic band-gap fibers with suppressed higher order modes and surface modes, J. Lightwave Technol. **25**, 2440 (2007).

[12] N. Y. Gordeev, A. S. Payusov, Y. M. Shernyakov, S. A. Mintairov, N. A. Kalyuzhnyy, M. M. Kulagina, and M. V. Maximov, Transverse single-mode edge-emitting lasers based on coupled waveguides, Opt. Lett. **40**, 2150 (2015).

[13] M. J. Li, X. Chen, A. P. Liu, S. Gray, J. Wang, D. T. Walton, and L. A. Zenteno, Limit of effective area for single-mode operation in step-index large mode area laser fibers, J. Lightwave Technol. **27**, 3010 (2009).

[14] L. Dong, X. Peng, and J. Li, Leakage channel optical fibers with large effective area, J. Opt. Soc. Am. B **24**, 1689 (2007).

[15] K. Peng, H. Zhan, L. Ni, X. Wang, Y. Wang, C. Gao, Y. Li, J. Wang, F. Jing, and A. Lin, Single-mode large-mode-area laser fiber with ultralow numerical aperture and high beam quality, Appl. Opt. **55**, 10133 (2016).

[16] M. Gong, Y. Yuan, C. Li, P. Yan, H. Zhang, and S. Liao, Numerical modeling of transverse mode competition in strongly pumped multimode fiber lasers and amplifiers, Opt. Express **15**, 3236 (2007).

[17] Y. Yuan, M. Gong, C. Li, and P. Yan, Theoretical and experimental study on transverse mode competition in a partial-coiled multimode fiber laser, Laser Phys. **18**, 52 (2008).

[18] Z. Hu, P. Yan, Q. Liu, E. Ji, and M. Gong, Transverse mode propagation studies in a thulium-doped fiber laser, J. Opt. Soc. Am. B **31**, 3181 (2014).

[19] A. V. Smith and J. J. Smith, Mode competition in high power fiber amplifiers, Opt. Express **19**, 11318 (2011).

[20] T. Eidam, C. Wirth, C. Jauregui, F. Stutzki, F. Jansen, H.-J. Otto, O. Schmidt, T. Schreiber, J. Limpert, and A. Tünnermann, Experimental observations of the threshold-like onset of mode instabilities in high power fiber amplifiers, Opt. Express **19**, 13218 (2011).

[21] C. Jauregui, T. Eidam, H.-J. Otto, F. Stutzki, F. Jansen, J. Limpert, and A. Tünnermann, Physical origin of mode instabilities in high-power fiber laser systems, Opt. Express **20**, 12912 (2012).

[22] A. V. Smith and J. J. Smith, Overview of a steady-periodic model of modal instability in fiber amplifiers, IEEE J. Sel. Top. Quantum Electron. **20**, 472 (2014).

[23] L. A. Lugiato, L. M. Narducci, E. V. Eschenazi, D. K. Bandy, and N. B. Abraham, Multimode instabilities in a homogeneously broadened ring laser, Phys. Rev. A **32**, 1563 (1985).

[24] L. A. Lugiato and L. M. Narducci, Single-mode and multimode instabilities in lasers and related optical systems, Phys. Rev. A **32**, 1576 (1985).

[25] A. E. Siegman, Propagating modes in gain-guided optical fibers, J. Opt. Soc. Am. A Opt. Image Sci. Vis. **20**, 1617 (2003).

[26] Y. Y. Liu, L. W. Casperson, and T. H. Her, Transverse mode competition in index-antiguided waveguide lasers, Appl. Phys. Lett. **107**, 241111 (2015).

[27] L. W. Casperson, Laser power calculations - sources of error, Appl. Opt. **19**, 422 (1980).

[28] C. Wang, Y. Liu, L. W. Casperson, and T.-H. Her, Power characteristics of planar index-antiguided waveguide lasers with transverse mode competition, AIP Adv. **6**, 125206 (2016).

[29] C. Wang, T.-H. Her, and L. W. Casperson, Power characteristics of homogeneously broadened index-antiguided waveguide lasers, Opt. Lett. **37**, 815 (2012).